7 Non-rotationally symmetrical surfaces: Toroidal surfaces

Now that the experimental setup has been tested and calibrated, and its measuring capability has been presented in Section 6, where the main features of the measurement technique were tested while developing spherical surface topographies, we are ready to start measuring radii of curvature and topographies of surfaces lacking the high degree of symmetry present in spherical surfaces.

Toroidal surfaces were chosen as examples of non-rotationally symmetrical surfaces. They have two circular sections (the so-called principal meridians) placed on the surface in orthogonal directions, so two different radii of curvature values will be measured. Incidentally, although the parametric equations that describe the toroidal

surface are well known, they are very hard to combine in practice in order to perform a three-dimensional fitting procedure. These procedures will be carried out using the spherocylindrical surface geometry, which is a very good approximation to the toroidal surface under our experimental conditions [Menchaca 1986]. Toroidal and spherocylindrical surfaces will be presented and compared in Section 7.1, where the toroidal surface samples which will be measured and the experimental procedures applied to them will also be described.

Section 7.2 will show a typical measurement process on one of the toroidal samples in a given position, as we did previously for spherical surfaces in Section 6.2. Due to the sample's lack of rotational symmetry, in toroidal samples measurements will be performed at four different orientations of the sample, with a tilt increment of the surface of 30° around the Z axis. The information provided in this Section 7.2 has been kept to a minimum, presenting only the features characteristic of the toroidal surface which contain information not available in the typical measurement of a spherical surface (Section 6.2).

In Section 7.3 complete results and conclusions for the six measured toroidal samples will be presented, showing the Ronchi test's ability to perform surface topographies and radius of curvature measurements of non-rotationally symmetrical surfaces. As in the case of spherical samples, combining the topographies performed using the Ronchi test with the numerical abilities of modern software packages will provide interesting residual plots when subtracting the best fitted spherocylindrical surface.

7.1 Sample surfaces

Though these are commonplace surfaces in our everyday life (forms of toroidal surfaces can be seen in anything from doughnuts to beer barrels), the lack of rotational symmetry of toroidal surfaces makes their mathematical description more complex than the perfect one obtained for a sphere, with its rotational symmetry and its equivalence of X, Y and Z axes.

This complexity (especially when talking of a unique expression in Cartesian coordinates valid in all points in space, needed to perform three-dimensional fitting

procedures) will be shown in Section 7.1.1. In Section 7.1.2 an approach designed to avoid this complexity will be proposed in the form of the spherocylindrical surface, which will also be described and compared to the toroidal surface. Finally, in Section 7.1.3 the toroidal samples which will be measured are presented following the pattern used in Section 6.1.

7.1.1.- Toroidal surfaces.

A toroidal surface is obtained by rotating a circle, with radius of curvature *b*, around an axis of symmetry placed a distance *a* away from the center of the circle, with the axis of symmetry contained in the same plane as the circle. Under this geometry, two radii of curvature placed in orthogonal directions may be measured on the surface: one coincides with the radius of the circle and the second is the sum of the radius of the circle and the distance from the center of the circle to the rotation axis. Doughnut-shaped toroidal surfaces are obtained if a>b; barrel shaped ones are obtained if a<b. a=b gives a spherical surface.
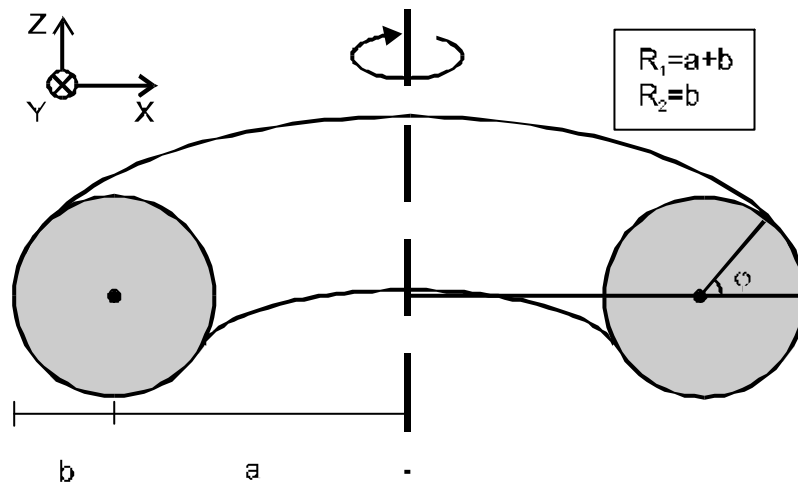

Fig. 7.1.1.: Toroidal surface.

The main feature of a toroidal surface thus becomes the presence of two circular sections placed orthogonally and crossing at the vertex of the surface. If we cut sections of the toroidal surface containing the vertex of the surface in all the intermediate positions between these circular sections, we would not obtain circular sections. That is, the transition between circular sections is accomplished through non-

circular curves. Only two radii of curvature, placed orthogonally along the only two circular sections present on the surface, may be obtained.

These two circular sections are called the principal meridians of the toroidal surface. The principal meridian with a flatter curvature is called the surface *base* curve, while the most curved one is called the *cross* curve of the toroidal surface. Obviously, the radius of curvature of the cross curve (R_C) will be smaller than the radius of curvature of the base curve (R_B) [Jalie 1980].

Our aim now is to find an expression that is valid in the whole spatial domain to describe the toroidal geometry in order to perform three-dimensional curve-fitting procedures. From Fig.7.1.1, it seems that a cylindrical coordinate system would be the best suited for the description of the toroidal surface. A toroidal surface with its rotation axis placed along the Z axis would be

$$x = (a + b\cos\varphi)\cos\theta$$
$$y = (a + b\cos\varphi)\operatorname{sen}\theta \qquad\qquad (7.1.1)$$
$$z = b\operatorname{sen}\varphi$$

using a cylindrical coordinate system where θ is the polar coordinate placed on the XY plane and φ the angular value shown in Fig.7.1.1. Parameters a and b were also defined in Fig. 7.1.1.

Incidentally, we would rather obtain an expression for the toroidal surface using Cartesian coordinates, which are better suited to the results obtained using the Ronchi test when placing its lines in orthogonal directions. The parametric nature of Eq. 7.1.1 is also not well suited to the curve-fitting procedures which gave such good results in Section 6, as the sign ambiguities caused by the trigonometric terms that appear in the process prevent direct conversion of Eq.7.1.1 to a z=f(x,y) function.

It can be shown [Malacara 1981] that a toroidal surface may be expressed in Cartesian coordinates as

$$\left[(x+a+b)^2 + y^2 + z^2 + a^2 - b^2\right]^2 = 4a^2\left[(x+a+b)^2 + y^2\right] \qquad\qquad (7.1.2)$$

where a and b are the distances described in Fig. 7.1.1. However, this Cartesian expression contains a degree of ambiguity hidden in the double sign of the square roots that appear in the expression when trying to obtain a z=f(x,y) description. This ambiguity introduces different mathematical expressions in different regions of the spatial domain, which prevent this expression from being useful in curve-fitting procedures. It is recalled that in the case of spherical surfaces, the usual description using

7.4

$$x^2 + y^2 + z^2 = R^2 \qquad (7.1.3)$$

was not used for this reason, being preferred instead

$$z = \frac{\dfrac{x^2 + y^2}{R}}{1 + \sqrt{1 - (\dfrac{x^2 + y^2}{R^2})}} \qquad (7.1.4)$$

(Eq. 6.2.1 with $x_0 = y_0 = 0$), which is defined at all points in space. We will thus be looking for a description of the toroidal surface in Cartesian coordinates valid for all regions in space, resembling Eq. 7.1.4.

An alternative description of the toroidal surface has still been found, and requires us to consider a geometry like that of Fig. 7.1.2 [Genii 1992]. This solution was obtained from the reference guide of an optical system design software (Gennesee++), where these surfaces were described in order to present the parameters needed in order to perform ray-tracing procedures through them. In this figure, however, it must be noted that the rotation axis of the toroidal surface is placed along the Y axis, and that the toroidal surface has been placed in the first spatial octant (the one with x>0, y>0 and z>0).

With the geometry of Fig.7.1.2, it may be shown that the toroidal surface is described through

$$x = x_0 + x_1 \cos \alpha$$
$$y = y_0 - x_1 \cos \alpha$$
$$f_y(x_0, y_0) = x_0 - \frac{C_Y y_0^2}{1 + \sqrt{1 - C_Y^2 y_0^2}} = 0 \qquad (7.1.5)$$
$$f_z(x_1, z) = x_1 - \frac{C_Z z^2}{1 + \sqrt{1 - C_Z^2 z^2}} = 0$$
$$\operatorname{tg} \alpha = -\frac{\partial f_y}{\partial y_0}$$

which comes back to a parametric expression not useful in curve fitting procedures, as obtaining a z=f(x,y) expression from this set of equations is extremely difficult. C_Y and C_Z stand for the curvatures along the two orthogonal sections of the toroidal surface. Even if this kind of expression was established, some sign ambiguity entailing division of the spatial domain would remain in the expression, as $\sin \alpha$ and $\cos \alpha$ should be

obtained from the known value of tgα. Once again, no z=f(x,y) expression for the toroidal surface which could be applied in the whole spatial domain was available.

Fig. 7.1.2: Cartesian description of the toroidal surface placed in the first spatial octant [Genii 1992]

To sum up, it was not possible to obtain a z=f(x,y) mathematical expression that was valid in the whole space for the toroidal surface. Our three-dimensional fitting procedures need such an expression to perform, so in order to provide three-dimensional topographies and residuals comparable to those presented in Section 6, a different approach has to be taken. This approach will be the spherocylindrical surface.

7.1.2.- Spherocylindrical surfaces.

Spherocylindrical surfaces were proposed as an alternative to toroidal surfaces, because of their simpler mathematical description and closeness to the toroidal shape near the surface vertex [Menchaca 1986]. They are also commonplace in many commercial lens design programs, as ray-tracing procedures through toroidal surfaces are quite complex to perform due to the mathematical description of the surface.

Spherocylindrical surfaces are described by [Malacara 1992]

$$z = \frac{C_X x^2 + C_Y y^2}{1 + \sqrt{1 - \frac{\left(C_X x^2 + C_Y y^2\right)^2}{x^2 + y^2}}} \qquad (7.1.6)$$

where again C_X and C_Y stand for the curvatures along the two orthogonal sections of the spherocylindrical surface. This expression which is very well suited to our three-dimensional curve fitting procedures, as it describes the surface in the whole spatial domain and is expressed in Cartesian coordinates. Spherocylindrical and toroidal surfaces with equivalent curvatures have coincident orthogonal circular sections, but make different transitions from one circular section to the other.

In order to estimate the amount of error introduced when approximating a toroidal surface using Eq. 7.1.6., both surfaces were calculated using parameters close to the ones obtained in our experimental setup. A spherocylindrical surface and a toroidal surface with two radii of curvature with values of 150mm for the cross curve and 200mm for the base curve were calculated in a 20x20mm section centered at the surface vertex. These radii of curvatures and sample areas are typical values of our experimental setup, as has already been shown in Section 6. Both surfaces were placed with their circular sections along the X and Y axes.

Fig.7.1.3 presents the deviation from the toroidal surface of a spherocylindrical surface. The contour labels are expressed in nm, so the contour steps were fixed at 10nm. In this calculated area of 400mm^2, the maximum deviation stays under the 0.1µm range at the edges of the sampling area. This value may be neglected under our experimental conditions, as the height variations being measured remain around 0.1mm, that is, a thousand times greater than the maximum deviation to be expected at the edge of the 20x20mm sample area.

In order to provide further proof of the equivalence of using spherocylindrical and toroidal surfaces, the same theoretical toroidal and spherocylindrical surfaces of R_B=200mm and R_C=150mm were three-dimensionally curve fitted using the spherocylindrical surface description. The numerical results for the radii of curvature obtained are presented in Table 7.1.1, where values for the position of the vertex and the tilt of the surface happened to be null, as could be expected from a theoretical surface. The residuals of the fitting for both cases were plotted in Fig. 7.1.4.

Fig. 7.1.3: Deviations of the spherocylindrical surface from the toroidal surface. Contour label increment 10nm.

Table 7.1.1: Radius of curvature values for two theoretical spherocylindrical and toroidal surfaces fitted to a spherocylindrical surface.
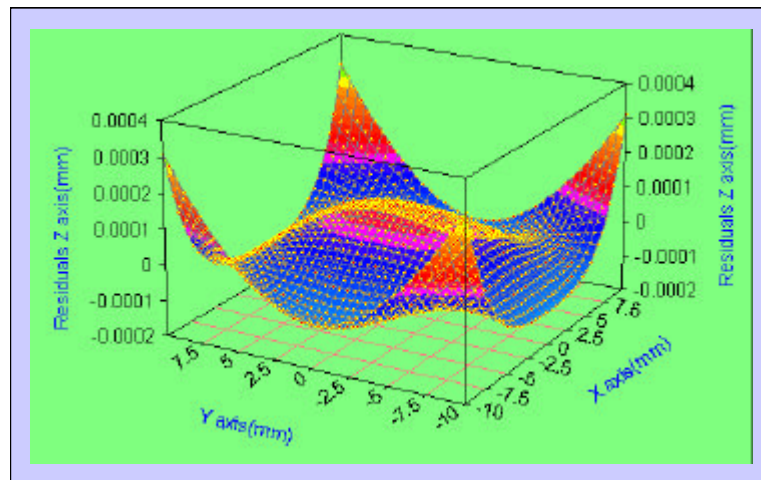
Surface	R_B(mm)	R_C(mm)	r^2
Theoretical	200.00	150.00	1
Spherocylindrical	199.85	150.02	0.99999980
Toroidal	199.83	150.00	0.99999974

Fig. 7.1.4: Residual plots of the fit to a spherocylindrical surface: a)Theoretical spherocylindrical surface; b) Theoretical toroidal surface.

(a)
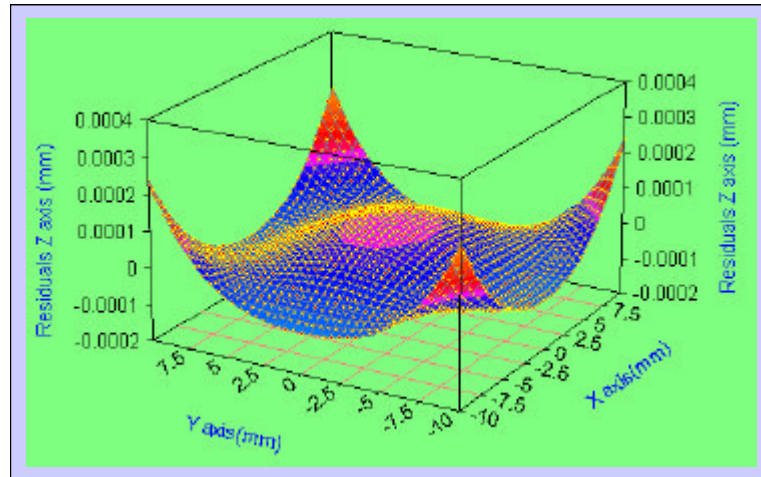
(b)

The fitted radius of curvature values may be considered equivalent, as may the correlation coefficients of the fit. A perfect correlation is not achieved even on these theoretical surfaces, because of the unavoidable rounding errors embedded in the software algorithms. These errors may be identified in the residual plots, which present a soft centered peak coincident with the lower values on X and Y axes. Both residual plots can be seen to be almost equivalent, the residual of the toroidal surface being slightly higher at the edges of the sampled area. The difference of the residual values

was plotted in Fig.7.1.5, showing that the maximum difference of the residuals amounts to 30nm in the measured area, and, once more, is only attained at its edges. However, in most of the considered area (at least in a 16x16mm area) the difference of the residuals remains under 10nm, a value which will allow us to consider spherocylindrical surfaces as being equivalent to toroidal ones under our experimental conditions.

Fig. 7.1.5: Differences of the residuals in Fig. 7.1.4. Contour label increment 5nm.

Spherocylindrical surfaces will thus allow us to obtain both radii of curvature of the surface with three-dimensional procedures, and calculate the topographies and residuals of toroidal surfaces following similar guidelines to the ones in Section 6.

7.1.3.- Toroidal samples.

7.10

The main difference found in toroidal samples when compared to spherical ones is their lack of rotational symmetry. This means that measurements are dependent on the position of the sample considered. In order to show how measurements are affected by the rotation of the sample, topographies were developed for four different orientations of the sample, which will be named G00, G30,G60 and G90. The base curve was placed along the X axis in the G00 orientation, and then tilted in 30° increments, leaving the cross curve along the Y axis in G90 orientation after the third tilt. This arrangement enables measurements to be performed in two orientations of the sample with their principal meridians placed in the same direction as the lines on the ruling (G00 and G90), and two orientations of the sample with its principal meridians tilted 30° and 60° from the lines on the ruling (G30 and G60).

As we will also be interested in studying the effect of translating the toroidal sample, topographies will be performed at three different distances of the sample from the Ronchi ruling, as we did previously when measuring spherical samples. This means twelve topographies per sample, with their corresponding residuals and fits, which is a vast amount of information. In order to keep the amount of information presented within reasonable limits, all non-microstepped measurements will not be presented, as the features of non-microstepped toroidal surface topographies are equivalent to the ones observed while developing spherical surface topographies.

As in Section 6, the samples will be obtained using the concave surface of ophthalmic lenses with their convex surface made optically inactive through grinding and painting. In this case lenses will obviously be toric and their concave surface will have a toroidal shape. Two different radii of curvature need now be measured at each sample.

As the surfaces are toroidal, the Möller-Wedel Combination V radioscope measurements will be provided only as an additional validation of the measured radius of curvature, because when measuring toroidal surfaces the instrument lacks the accuracy that it had for spherical surface measurements. The reference radii of curvature presented in Table 7.1.2 are assumed to have an uncertainty of ±1.0mm.

Samples will now be named after their spherocylindrical expression, which takes into account a combination of the two back vertex powers available in the toric lens. Three pairs of nominally identical lenses will be tested, as in the case of spherical samples, in order to present the technique's potential for making high precision

measurements. The different d_R distances from the sample to the Ronchi plane are presented in Table 7.1.2.

The range of d_R distances involved in our experiments is even smaller than the one used when measuring spherical surfaces, as to obtain good quality topographic measurements we need a high enough number of bright lines in each acquired ronchigram. This number of lines depends on the d_R distance and on the radius of curvature of each of the principal meridians. At a given d_R distance, the number of bright lines visible in the ronchigram with the ruling lines placed along the X axis may be very different from the number of bright lines of the ronchigram with ruling lines placed along the Y axis, depending on the difference of radius of curvature of both principal meridians of the toroidal surface. This reduces the range of d_R distances where ronchigrams may be acquired with enough bright lines in both orthogonal positions of the lines on the ruling.

Table 7.1.2: Name, back vertex power of the base curve ([BVP]$_B$) and the cross curve ([BVP]$_C$), radii of curvature obtained using the Möller-Wedel radioscope (R_B and R_C) and distances to the Ronchi ruling (P1,P2 and P3) of the toroidal surfaces used as samples.

Name	[BVP]$_B$ (D)	[BVP]$_C$ (D)	R_B (mm)	R_C (mm)	P1 (mm)	P2 (mm)	P3 (mm)
P30025A	3.00	3.25	172.0	159.7	186.7	192.2	193.4
P30025B	3.00	3.25	172.6	160.6	186.8	192.3	193.4
P30050A	3.00	3.50	170.9	148.8	180.1	182.6	188.4
P30050B	3.00	3.50	169.7	147.7	180.0	182.6	188.4
P45075A	4.50	5.25	201.4	159.8	211.3	215.3	220.6
P45075B	4.50	5.25	202.7	158.0	211.3	215.3	220.6

7.2 Typical measurement example

Although the data processing steps and the experimental setup are exactly the same as the ones used for obtaining spherical surface topographies and the same procedures and algorithms are applied, in toroidal surfaces the lack of rotational symmetry of the samples involves significant differences from spherical surfaces in the measurement process. These differences will be presented in this Section 7.2, together with an error analysis of the results (Section 7.2.2) and a comparison of the radius of curvature values obtained with the reference values (Section 7.2.3)

Only microstepped results will be presented, as non-microstepped measurements follow equivalent guidelines to the ones given in Section 6.2; that is, the radius of curvature of the surface may be measured accurately in non-microstepped measurements, but the surface topographies obtained are quite poor when compared with the corresponding microstepped one. Also ten ronchigrams in each direction will be recorded for toroidal samples, providing a measurement process independent of the rotational symmetry of the surface.

7.2.1.- Measurement of sample P30025A in position P1

As in the case of spherical surfaces, the sample P325A in position P1 measurement was chosen arbitrarily as an example, since the features presented are fully equivalent to the ones observed in other samples, except for some numerical values and for the number of fringes that can be observed in the ronchigrams.

Obviously, the major difference from spherical samples will be the variation in the ronchigrams when the sample is tilted. As with the remaining samples and positions, four orientations were measured tilting the surface in 30° increments. At tilts G00 and G90 the principal meridians of the surface are placed along the X and Y axes, and subsequently placed in the same direction of the lines on the ruling. However, in the G30 and G60 intermediate tilts the principal meridians are not aligned with the lines on the ruling. For the first time, the lines on the ruling are not placed in the direction of any circular section of the sample surface. One tilt of each of the two groups was chosen in order to illustrate the measuring process of a toroidal surface: the G90 tilt will stand for the group of experiments with principal meridians placed in the same direction as the ruling lines, and the G60 tilt will stand for the group of ronchigrams with principal meridians not aligned with X and Y axes.

In Fig. 7.2.1 the reference ronchigrams along both axes are presented for both tilts, while Fig. 7.2.2 shows the first pair of ronchigrams used as data. As previously explained, all presented results correspond to microstepped data, so this pair of ronchigrams is the first in a series of ten pairs in both tilts of the surface, with the ruling lines displaced T/10 along X and Y axes.

Fig. 7.2.1: Reference ronchigrams a) Ruling lines along the X axis, G90 tilt; b) Ruling lines along the X axis, G60 tilt; c) Ruling lines along the Y axis, G90 tilt; d) Ruling lines along the Y axis, G60 tilt.
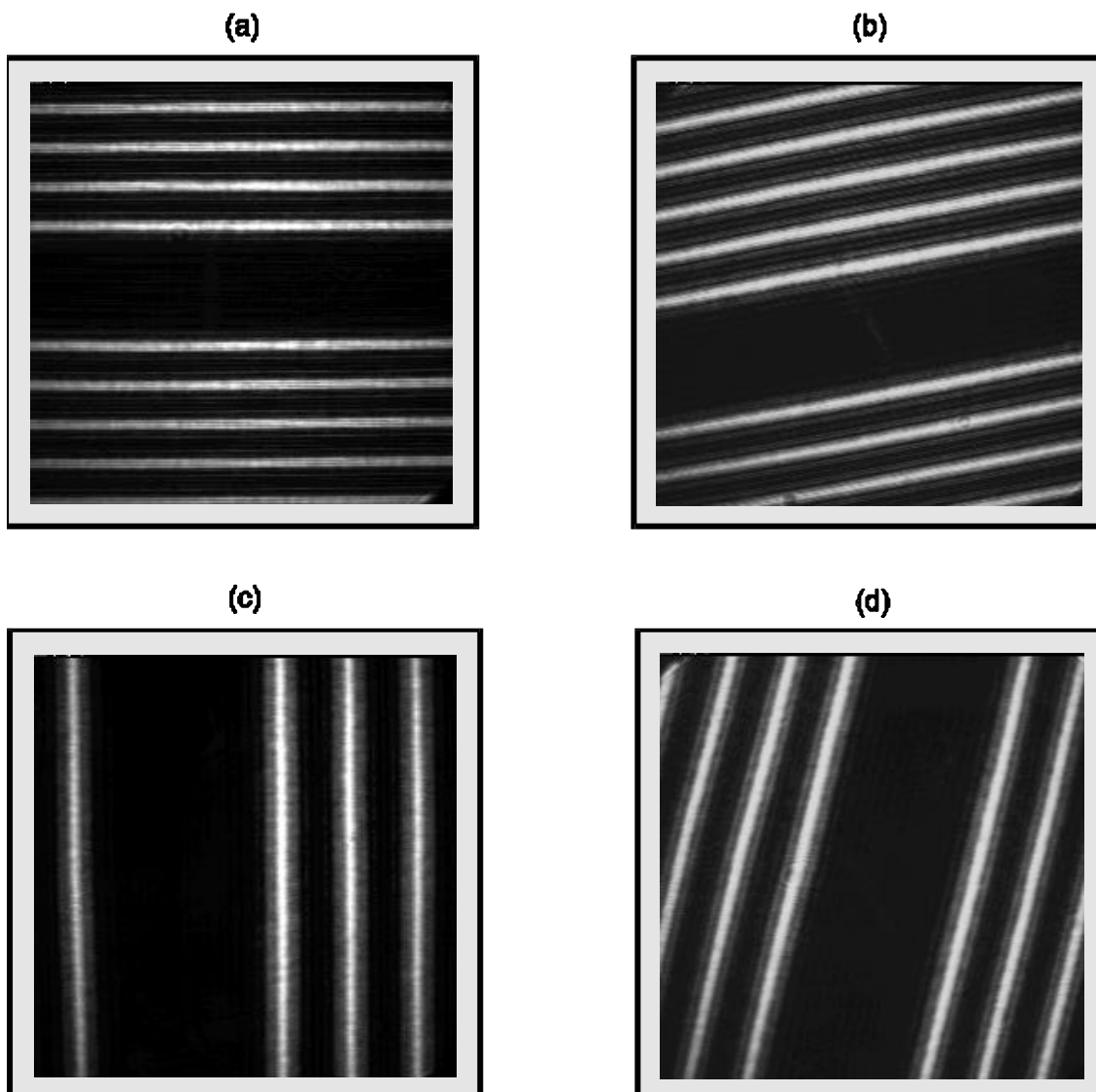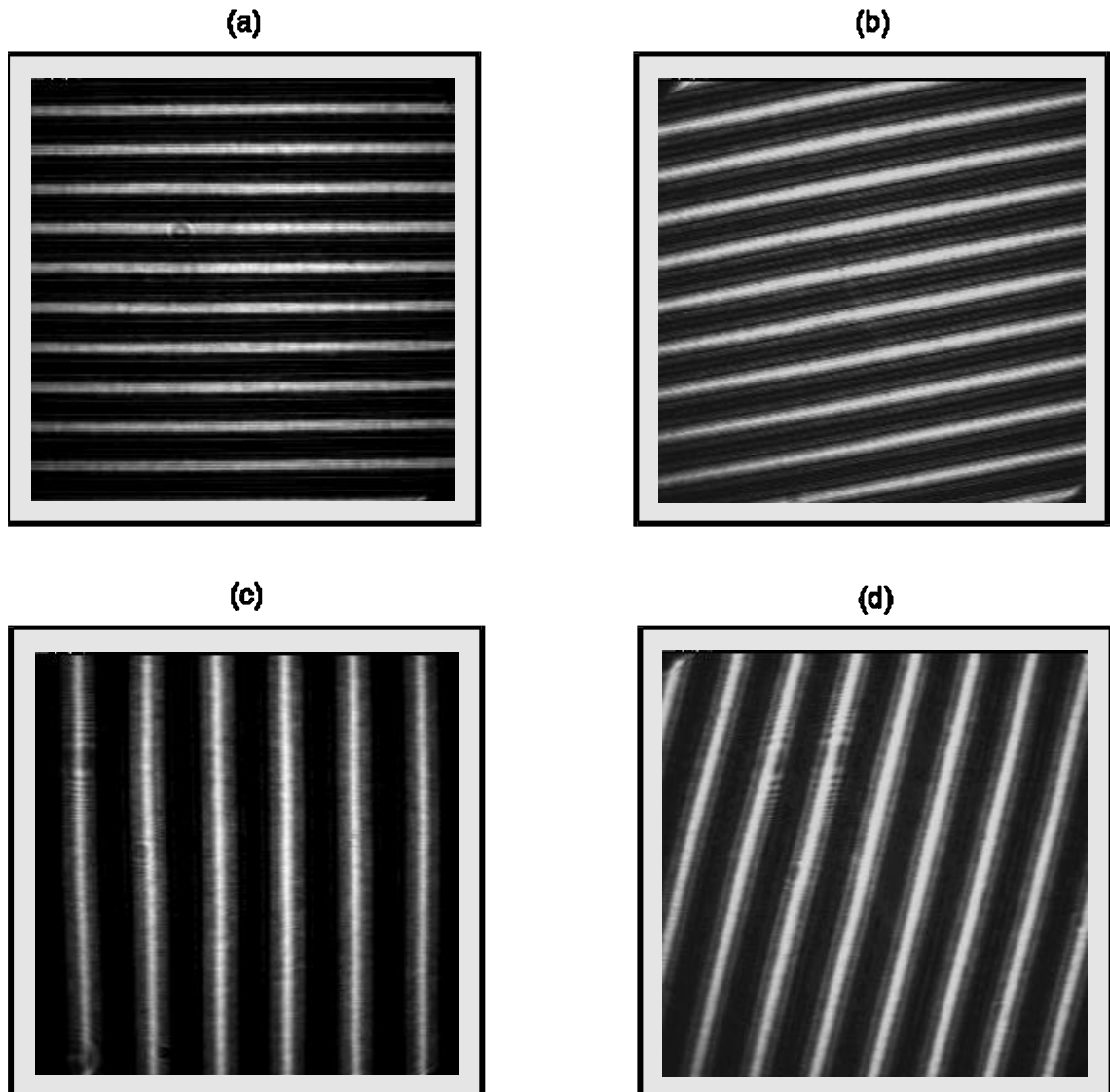
Fig. 7.2.2: First pair of acquired ronchigrams a) Ruling lines along the X axis, G90 tilt; b) Ruling lines along the X axis, G60 tilt; c) Ruling lines along the Y axis, G90 tilt; d) Ruling lines along the Y axis, G60 tilt.

(a)

(b)

(c)

(d)

Relevant differences from spherical surfaces can be easily observed in Fig. 7.2.1 and Fig.7.2.2. While in spherical surfaces the number of bright lines present in the ronchigrams with ruling lines along X and Y axes were the same (with maximum differences of one fringe, depending on the position of the ruling), in toroidal surfaces a different number of bright lines in each ronchigram should be expected from the different curvatures present at each principal meridian. The effect becomes more evident in the ronchigrams corresponding to the G90 tilt, while in the G60 tilt the effect is slightly reduced as the principal meridians are not aligned with the directions of the lines

on the ruling. This difference in the number of bright lines will be greater as the difference between orthogonal radius of curvature values increases. This has been confirmed when performing measurements on samples P30050A, P30050B, P45075A and P45075B, which have a bigger difference in the radius of curvature of their principal meridians.

However, the most clearly visible novelty compared with spherical surfaces is the rotation of the shadows of the lines in the G60 tilt. We again point out that the Ronchi ruling lines were placed following X and Y axes, in the same way as in the G90 tilt or in the spherical samples. However, the shadows of these orthogonal lines, recorded in the ronchigrams, are no longer orthogonal. This is a consequence of the lack of coincidence of the Ronchi ruling lines with the principal meridians, that is, the circular sections of the toroidal surface. The behavior of the G30 tilt is equivalent to G60 (with different tilt angle of the lines in the ronchigrams), as the principal meridians do not follow X or Y axes, either. The G00 tilt behaves like the G90 tilt, with the number of bright fringes changed in the ronchigrams with ruling lines along X and Y axes, as should be expected from the ronchigrams of a surface which has been rotated 90°.

The set of twenty ronchigrams recorded for each of the G90 and G60 tilts are then processed in the same pattern, and with the same algorithms and software programs as were used for spherical surfaces. All ronchigrams are smoothed, binarized and eroded yielding results similar to the ones presented in Section 6.2. A final set of twenty one-pixel-wide line patterns are obtained.

Superposition of these line patterns will give the complete set of intersection points where the set of (x_R, y_R, u, v) data is measured. The superposition of eroded ronchigrams for both tilts of the sample are presented in Fig.7.2.3. Notice how, although the lines are not orthogonal in Fig.7.2.3b, microstepping procedures may be performed in the same way, as the ruling is displaced along the X or Y axis and the ronchigram lines will be displaced by the same amount, T/10 in our case, regardless of their orientation.

Once the wavefront has been sampled on the Ronchi ruling plane, it is possible to build the $y_R(x_R)$, $u(x_R)$ and $v(y_R)$ plots for each of the tilts of the sample. These plots are presented in Fig. 7.2.4., and again display interesting differences when compared to those of spherical samples.

7.16

Fig. 7.2.3: Superposition of eroded ronchigrams (a) G90 tilt; (b) G60 tilt.

(a)   (b)
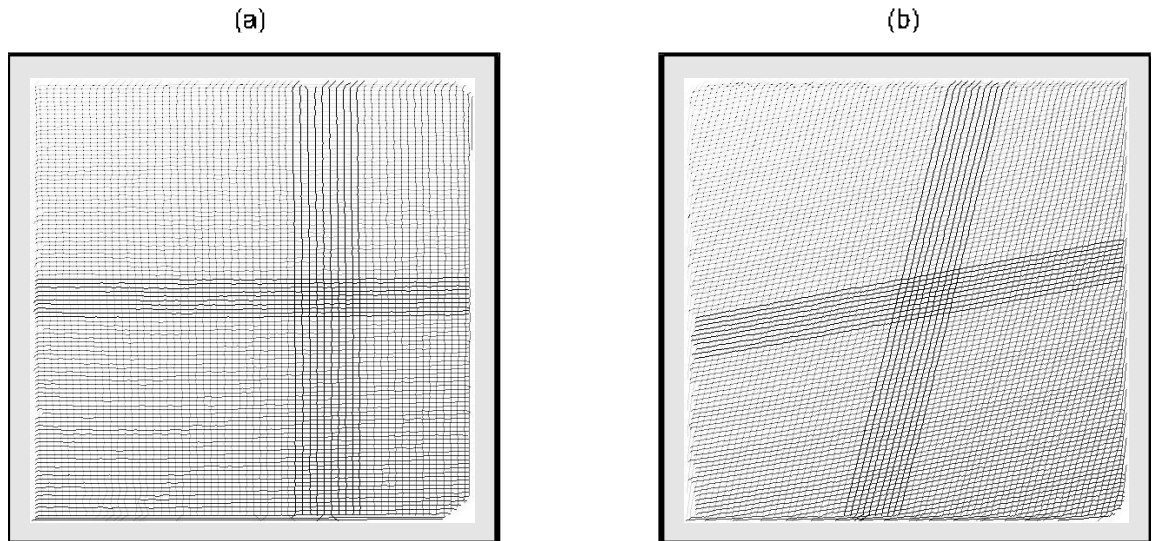
Both x_R and y_R axes were intentionally fixed at the same length (8mm) to allow direct comparisons between both coordinates at both angular tilts, although this means that data will not be centered in each graph. Subplots (a), (c) and (e) correspond to the G90 tilt, while (b), (d) and (f) belong to the G60 tilt measurement.

The $y_R(x_R)$ plots in both positions confirm our previous comments on toroidal samples. The different number of lines along each direction in the ronchigrams makes the area sampled take a rectangular shape in Fig. 7.2.4a, instead of the quasi-square shapes typical of spherical surfaces. When the lines in the ronchigram do not follow the directions of the lines on the ruling, the sampled area has the diamond-like shape of Fig.7.2.4b.

However, the key difference when measuring with the ruling lines placed along the principal meridians of the surface (as in G90) or with the ruling lines placed along a section of the surface which is not circular may be seen in the $u(x_R)$ and $v(y_R)$ plots. In the G90 tilt we find sections of the surface close to the circular shape along the X and Y axis, so theoretical straight lines whose slope is the curvature of the wavefront may be expected, if a toroidal shape of the wavefront is assumed at the Ronchi ruling plane. However, if we are considering a section of the toroidal wavefront other than the principal meridians, the $u(x_R)$ and $v(y_R)$ plots should have noticeable variations from the linear shape.

7.17

Fig. 7.2.4c and 7.2.4e may be seen to be linear data plots, as expected, as they correspond to the G90 tilt. They can be seen to present different slope values, reflecting the different curvatures along the principal meridians placed on each axis. Fig 7.2.4d and 7.2.4f present a cloud of data points which cannot be regarded as a single line, showing how the sections of the toroidal wavefront placed along the X and Y axes are not circular ones. In Fig. 7.2.5 we present the sections of these measured data along the 60° and 150° directions, where the principal meridians of the surface are supposed to be placed. The plots may be seen to appropriately fit a linear shape, as we are now plotting slope against position along a circular section of the surface, and with different slopes, as the incident wavefront was assumed to be toroidal. In order to differentiate them from Fig. 7.2.4d and 7.2.4f, these plots will hereafter be named $u^{60}(x_R^{60})$ and $v^{60}(y_R^{60})$, as they were obtained through a 60° rotation of the experimental data in Fig.7.2.4.

Table 7.2.1: Linear regression results for the curves corresponding to the G90 and G60 tilts, and to the circular sections of the G60 tilt measurement . A curve $y = C\xi + K$ was fitted with ξ being either x_R, y_R, x_R^{60} or y_R^{60}. y may be either u, v, u^{60} or v^{60}. C stands for curvature, K for angular misalignment, r^2 for the correlation coefficient and R for the measured radius of curvature of the wavefront on the Ronchi ruling plane.

Sample P30025A		C(mm^{-1})	K(rad)	r^2	R(mm)
G90	$u(x_R)$	-3.3858 10^{-2}	-0.0247	0.99975	29.54
	$v(y_R)$	-2.0939 10^{-2}	0.0422	0.99993	47.76
G60	$u(x_R)$	-2.7552 10^{-2}	0.0226	0.94128	36.29
	$v(y_R)$	-2.2445 10^{-2}	-6.48 10^{-3}	0.96791	44.55
G60	$u^{60}(x_R^{60})$	-3.4137 10^{-2}	-0.0289	0.99984	29.29
rotated	$v^{60}(y_R^{60})$	-2.0870 10^{-2}	3.49 10^{-3}	0.99984	47.91

Two-dimensional fitting results are presented in Table 7.2.1. The shadowed rows are the poor quality fits corresponding to Fig.7.2.4d and Fig.7.2.4f, that is, to slope against position fits along directions of the surface other than its principal meridians. Their r^2 coefficient is quite bad, and the curvature values obtained will not

Fig. 7.2.4: Measured data of the reflected wavefront at the Ronchi ruling; (a) $y_R(x_R)$ for the G90 tilt; (b) $y_R(x_R)$ for the G60 tilt; (c) $u(x_R)$ for the G90 tilt; (d) $u(x_R)$ for the G60 tilt; (e) $v(y_R)$ for the G90 tilt; (f) $v(y_R)$ for the G60 tilt.